Available online at www.sciencedirect.com

SCIENCE DIRECT®

European Journal of Mechanics B/Fluids 24 (2005) 425–438

Velocity scales in the near-wall layer beneath reattaching turbulent separated and boundary layer flows

P.E. Hancock

Fluids Research Centre, School of Engineering, University of Surrey, Guildford, Surrey GU2 7XH, UK

Received 9 December 2003; received in revised form 4 August 2004; accepted 18 October 2004

Available online 18 January 2005

Abstract

This paper investigates the idea that each Reynolds stress has its own velocity scale – the mean shear stress cannot provide a velocity scale for the near-wall turbulence near reattachment, for example, and cannot by definition provide a velocity scale for 'inactive' motion. Beneath a separation bubble, the tangential velocity fluctuations scale on the r.m.s. of the respective wall shear stress fluctuation and on ν/y, which is the viscous velocity scale in the usual way, independent of the other flow. This paper also shows that the wall-normal direct stress and the shear stress have respective, independent velocity scales. Moreover, and quite remarkably, the scaling functions for these latter stresses appear to be universal in that they are unchanged for the boundary layer upstream of separation or downstream of reattachment, and are as in the canonical zero-pressure gradient boundary layer. The streamwise direct stress does not exhibit this universality, raising questions about the near wall structures: it is inferred that the change in form is associated with the disappearance and reappearance of the streak-like structures.

Keywords: Turbulent separated flow; Near-wall layer; Turbulent boundary layer

1. Introduction

Gaining an understanding of the scaling laws for turbulent motion is a fundamental step in gaining an understanding of the complex structures that makes up that motion. It is also the case that gaining an understanding of the structures should assist in gaining an understanding of the scaling laws. Historically, because the scaling laws involve only ensemble-averaged quantities and involve relatively much more straightforward measurement techniques (or analysis from Large Eddy or Direct Numerical Simulation) and less of a conceptual challenge, attention to scaling laws has by and large preceded attention to structures.

Much effort has been given to the scaling of the "canonical" zero-pressure-gradient two-dimensional flat plate boundary layer, but despite this questions still remain even for this 'basic' case. However, DeGraaff and Eaton [1] conclude fairly convincingly that in the inner layer $\overline{v^2}$ and $\overline{uv}$ do scale upon u_τ (defined as $\sqrt{\tau/\rho}$, where τ/ρ is the kinematic mean wall shear stress), but that $\overline{u^2}$ does not, scaling instead on a mixed velocity scale based the (product of) u_τ and the free-stream velocity. Here, u and v are, respectively, the velocity fluctuations in the streamwise and wall-normal directions, x and y. Their measurements are also supported by the recent measurements of Metzger et al. [2]. DeGraaff and Eaton did not measure the lateral fluctuation, w, and although both u and w are wall-parallel fluctuations it does not follow that $\overline{w^2}$ will exhibit a scaling like

E-mail address: p.hancock@surrey.ac.uk (P.E. Hancock).

0997-7546/$ – see front matter
doi:10.1016/j.euromechflu.2004.10.003

that for $\overline{u^2}$. Their results are opposite to the earlier conclusions of Fernholz and Finley [3] based an extensive review of measurements, namely, that $\overline{u^2}$ scales on u_τ and that there is some uncertainty as to whether $\overline{v^2}$ and $\overline{uv}$ (and also $\overline{w^2}$) scale on u_τ. The scaling of DeGraaff and Eaton does not alter the conclusion that the extent over which an inner layer scaling applies for the Reynolds stresses is markedly less than that for the mean velocity (U), the reasons for this remaining as yet unresolved. When, in the classical scaling framework, a boundary layer is subjected to, in particular, an adverse pressure gradient the streamwise and lateral Reynolds stresses ($\overline{u^2}$ and $\overline{w^2}$) are increased in relation to u_τ^2, but $\overline{uv}$ and $\overline{v^2}$ are in essence unchanged. Townsend [4] attributed this to 'inactive' motion driven by the more intense large-scale motion in the outer layer. Inactive motion is present in the canonical case but is much weaker, and it is interesting to note Robinson's [5] review summary that outer flow events have a definite but not controlling effect on the near-wall flow of the canonical layer. The influence of the free-stream velocity in the scaling of $\overline{u^2}$ [1] is, therefore, not all that surprising.

The present flow, that of a near-wall layer formed beneath the region of reattachment, is perhaps the most removed from that of the inner layer of a zero-pressure-gradient canonical boundary layer in that the outer flow is very much more intense and the layer itself newly developing rather than long established. Compared with the canonical layer relatively little is known about the structures in separated flow. The near-wall layer in both cases is characterised by a mean strain rate arising from the direct effect of viscosity on the velocity field, and the wall constraints on the turbulence, and so some similarity of structures might exist. However, Fernholz [6] and Na and Moin [7], for instance, show the near-wall layer to be dominated by impinging outer-layer structures, and Hancock [8] found the wall-shear stress fluctuations to be very nearly axisymmetric, implying no preferred alignment of structures, and determined primarily by the outer flow.

The consideration given in this paper is to the idea that, in the near-wall region, a separate velocity scale is needed for each Reynolds stress, and is done so primarily in the context of the layer beneath a reattaching separated flow, though some discussion of boundary layer flow is also given. No structure-function measurements were made. It was prompted by an analysis of measurements of Hardman [9] in the reattachment region of a three-dimensional separated flow. These strongly suggested that the tangential intensities, u' and w' ($=\sqrt{\overline{u^2}}$ and $\sqrt{\overline{w^2}}$) in the near-wall flow scale on velocities, u'_τ and w'_τ, formed from the r.m.s. of the wall shear stress fluctuations in the streamwise and lateral directions, respectively τ'_x and τ'_z. Specifically, they indicated that

$$\frac{u'}{u'_\tau} = f_u\left(\frac{u'_\tau y}{\nu}\right) \tag{1.1}$$

and

$$\frac{w'}{w'_\tau} = f_w\left(\frac{w'_\tau y}{\nu}\right), \tag{1.2}$$

where this behaviour existed beneath $u'_\tau y/\nu$ and $w'_\tau y/\nu$ of about 70, and over a fetch exceeding half a bubble length upstream and downstream from the attachment line. Moreover, (i) to within the measurement uncertainty, f_u and f_w were indistinguishably different from each other and (ii) exhibited a region of approximately logarithmic behaviour. (Some results regarding (1.1) were given in [10].)

Now, asymptotically, as $y \to 0$, u' and w' are related to τ'_x and τ'_z by

$$u' = y\frac{\tau'_x}{\mu} \quad \text{and} \quad w' = y\frac{\tau'_z}{\mu}$$

which can be written in non-dimensional form as

$$\frac{u'}{u'_\tau} = \frac{u'_\tau y}{\nu} \quad \text{and} \quad \frac{w'}{w'_\tau} = \frac{w'_\tau y}{\nu}.$$

These are, of course, true for any flow very near a surface. The proposition in this paper is that, beneath a separated flow, u' and w' in the near-wall layer depend only on, respectively, u'_τ, y and ν, and w'_τ, y and ν. This, is the simplest possible hypothesis, and requires that neither the mean flow nor the outer layer scales have any *explicit* parametric influence. Nevertheless, the outer layer is expected to have influence in that it is at least partly responsible for driving the velocity fluctuations in the near-wall layer (inactive motion). But, the proposition here is that y is sufficiently small compared with the length scale, L, of these structures that L is itself unimportant in the near-wall layer. Eqs. (1.1) and (1.2) follow. It is clear though, as will be demonstrated later, that Eq. (1.1) is certainly not generally true for all wall-bounded flows, and that f_u and perhaps f_w is a function of other flow parameters. The reasons for supposing that the mean flow in the near-wall layer might have no significant effect is the observation that streamwise and lateral gradients in mean velocity are very much less than they are in the viscous-dominated layer immediately adjacent to the surface, and the results of [8]. Those results showed that the mean shear $(\partial U/\partial y, \partial W/\partial y)$

at the surface had no effect on the r.m.s. of the wall shear stress fluctuations. Even so, it is to be expected that after some developmental length of the near wall layer, the gradient in mean velocity and the generation of $\overline{u^2}$ must become significant.

In extending the above line of argument it is supposed, prima facie, that the Reynolds normal stress arising from the vertical fluctuations, $\overline{v^2}$ and the shear stress, $\overline{uv}$ also have velocity scales, which we denote as v'_0 and s'_0. That is,

$$\frac{v'}{v'_0} = f_v\left(\frac{v'_0 y}{\nu}\right) \tag{1.3}$$

and

$$\frac{s'}{s'_0} = f_w\left(\frac{s'_0 y}{\nu}\right) \tag{1.4}$$

for some range of $v'_0 y/\nu$ and $s'_0 y/\nu$ as yet to be determined (i.e., from the surface to some outer point), where $s' = |\overline{uv}|^{1/2}$. Unlike, u'_τ and w'_τ, which are defined in terms of the (r.m.s. of the) wall shear stress fluctuations, v'_0 and s'_0 do not have a similarly easy physical interpretation, available from independent measurement. As a consequence v'_0 and s'_0 have therefore to be determined indirectly – that is from the profiles of v' and s' themselves, the necessary and sufficient condition being that v' and s' conform to Eqs. (1.3) and (1.4), independently of the outer flow, as will be discussed further in Section 3.

The pulsed-wire velocity probe as set up was only capable of making measurements of the fluctuations parallel to the surface. In principle, the probe could be set at an angle to the perpendicular to measure $\overline{v^2}$ and $\overline{uv}$, but this would be more difficult to achieve in practice (needing a new probe) and has not been attempted. To test the proposed idea for v' and s' we use the particularly careful measurements of $\overline{u^2}$, $\overline{v^2}$ and $\overline{uv}$ by Song et al. [11] who used a miniature LDA. However, they did not measure the wall shear stress fluctuations and so there is no independent check on u'_τ. Therefore, the approach here is to infer u'_τ (firstly) from measurements nearest the wall and (secondly, for three cases) from consistency further out with the present results. Obtaining u'_τ by extrapolation from the nearest measurements of u' is very demanding of the accuracy of these few points, and is something that has to be done with caution even for the mean shear stress in a standard boundary layer, for example, where the measurements are much easier to make. Several other sources of laboratory data were examined in the hope that the measurements would be accurate enough to infer velocity scales, but the very-near-wall data were far too scattered to obtain anything like a reliable r.m.s. of the wall shear stress fluctuation. As far as the author is aware no others sets exist for separated flows; there are a some limited measurements for boundary layer flows. The DNS of Le et al. [12] of a back-step flow is used, though the Reynolds number may be too low for proper comparison to be made. It is included here partly because this data set is quite often used as a reference.

In that no structure-function measurements were made it is not possible to make more than a few inferences here as regards structure. At and over a substantial fetch either side of reattachment the fluctuations in wall shear stress are very nearly axisymmetric [8], whereas in a canonical boundary layer the streamwise fluctuations are larger by a factor of roughly 1.4. Na and Moin's [7] DNS of separation and reattachment over a smooth wall show the streaky structures disappear upstream of separation, replaced by a much larger-scale near-wall structure showing little preferred direction beneath the bubble, and re-establishment of the streaky structures some distance after reattachment.

2. Experimental techniques

A two-dimensional separated flow was formed downstream of a sharp-edged, normal flat plate mounted centrally on the front of a horizontal splitter plate. The razor sharp edges of the normal flat plate were slightly uneven after manufacture and so were very slightly blunted (parallel to the horizontal) be means of a precision grinding machine to give an accurately controlled 'fence' height. Tip-to-tip, the normal flat plate height was 23.8 mm, and the plate thickness was 3.2 mm. The rig was supported by slender legs on the centre-plane of the wind tunnel working section, of height 500 mm, span 1.53 m and overall length 2.8 m. The splitter plate was made in two parts. The first, 500 mm in length, was aligned with the working section axis, while the second, 350 mm in length, formed a trailing edge flap, where the angle (of about 1° upwards) was controlled by adjusting the length of the supporting legs, to give equal bubble lengths on both surfaces. (A similar normal flat plate and splitter plate arrangement has been used in a number of other studies – see [13].) All the measurements were made at an upstream free stream speed, U_r, of 5.9 m/s, giving a Reynolds number based on h_f of 3900, where h_f is the 'fence' height of the tip above the splitter plate surface.

The distance to reattachment from separation, X, was 216 mm, implying a ratio of flow width to bubble length of 7. Ciampoli and Hancock [14] concluded that this ratio should not be less than 4 if significant end-wall effects were to be avoided, but that even at a ratio of 7 there are still residual end effects. However, any residual end effects are not particularly important here because our concern is to relate only the near-wall intensity to the r.m.s. of the wall shear stress fluctuations.

The probes were supported in a plug which in turn was held in a slot along the centreline of the first splitter plate, allowing a probe to be placed in the range $x = 22$ mm to 317 mm, the remainder of the slot being filled with blank plugs to give a smooth surface. The velocity in the near-wall layer was measured by means of a special 'near-wall' pulsed-wire probe similar to but smaller than the second probe of Schober et al. [15] – the pulsed- and sensor-wires where, respectively, parallel and perpendicular to the surface. The probe prongs were supported from beneath the plate surface and passed through small holes, the prongs and wires being moved as a whole by means of a micrometer head to a height accuracy of 0.01 mm. At the lowest position the pulsed wire touched the (electrically and thermally insulating) surface, and reached 13 mm at its highest. The wire lengths were about 6 mm in each case, and the pulsed- and sensor-wire diameters were 9 μm and 2.5 μm, respectively. Characteristics of the velocity probe are given by Hancock [16], but key points are given below.

The velocity probe was calibrated with it mounted close (70 mm) to the leading edge of a small, thin horizontal plate with a gently rounded leading edge, mounted ahead of the main flow rig. The probe was (i) close enough to the leading edge for it to be above the boundary layer at all speeds at its maximum travel, (ii) far enough from the leading edge to be free of its effects. A third-order polynomial was fitted to the velocity calibration in the usual way, but with careful attention to the calibration velocity intervals so as to give higher weight to the lower velocities and hence a comparable error as a fraction of the calibration velocity, over the whole range. In addition, two ranges were employed for these calibration fits: 0.4 to 6 m/s and 0.4 to 2 m/s, with the appropriate calibration curve selected (though not dynamically) according to the level of fluctuation. The errors between the curve and the calibration points were within the greater of ±0.07 m/s or ±4% for the first range and within the greater of ±0.03 m/s or ±2% for the second.

The pulsed-wire velocity probe gives a systematic error in regions of high velocity gradient as arise near the wall. This is because vertical thermal diffusion of the heat tracer leads to a faster convection and therefore earlier detection of the tracer. Castro and Dianat [17] first identified this behaviour, and a consistent correction given by Schober et al. [15] was extended to a method for high-intensity turbulent flow by Hancock [16], which showed the error was only significant below $u'_\tau y/\nu$ of 10 or less, and significant only below $u'_\tau y/\nu$ of 3 for some stations. The calibration for the effect of shear was achieved with the probe in the measurement position by requiring the *mean* wall shear stress as implied by the mean velocity to be consistent (in an iterative procedure) with the mean wall shear stress as measured by the pulsed-wire wall shear-stress probe. This amounts to defining an effective value for the parameter C in Schober et al. [15], which was taken as 6 in the measurements here. See [16] for further details, where it is demonstrated that this leads to the correct measurement of u' near $y = 0$ as implied by the (r.m.s. of the) wall shear stress fluctuations, this concurrence providing a check on the correction procedure.

As just mentioned the wall shear stress was measured by means of a pulsed-wire shear stress probe [18]. This was calibrated against a Preston tube [19], itself within ±2% of two other tubes of differing diameter, in a zero-pressure gradient turbulent boundary layer on the working section floor, and fitted by a third-order polynomial. The Preston tube calibration is itself accurate to about ±3% [19]. As for the velocity probe, the shear stress intervals were chosen so as to maintain accuracy at low shear stress, and again the fits were made over two ranges, ±0.2 Pa and ±0.08 Pa, with the range chosen according to the level of fluctuation. The error between the curve and the calibration points were within the greater of ±0.003 Pa or ±5% for the first range and within the greater of ±0.002 Pa or ±3% for the second. Like the error limits given earlier for velocity these are extreme limits of expected error; the actual errors are expected to be not more than about half these.

The lateral velocity, $W + w$, and the lateral wall shear stress, $\tau_z + \tau''_z$, were measured by rotating the respective probes to angles (θ) of ±45°, with mean and fluctuating quantities found in the normal way. That is, for W and $\overline{w^2}$

$$U_\theta = U\cos(\theta) + W\sin(\theta),$$
$$\overline{u^2}_\theta = \overline{u^2}\cos^2(\theta) + \overline{uw}\sin(2\theta) + \overline{w^2}\sin^2(\theta),$$

where U_θ and $\overline{u^2}_\theta$ are as measured by the probe at angle θ. The equations for the mean wall shear stress and the mean square of the shear stress fluctuation are of the same form, where the fluctuations τ''_x and τ''_z replace u and w, and the means τ_x and τ_z replace U and W, respectively. In the present measurements W and $\overline{uw}$ were zero, within the expected error band limits, as was $\overline{\tau''_x \tau''_z}$.

Both pulsed-wire probes were driven by a Pela anemometer, with control and data acquisition by means of LabView virtual instruments and a Macintosh computer. Pulse duration was 4 μs, sensor current 2 mA and gain and threshold were 2 and 0.5 V, or 1 and 0.5 V for the shear stress probe. The yaw responses for the velocity and shear stress probes were ±75° and ±85°, respectively, the latter implying negligible error.

The parameter ε in the error analysis of Castro and Cheun [20] was less than 0.03, and the associated errors in U and u' were within about ±2.5%. Sample periods were at least 5000 samples, at about 30 Hz, which was a rate low enough for consecutive samples to be statistically independent and amounted to about 5000 or more time scales based on bubble length and free stream velocity. Some measurements were made from 3000 samples at 10 Hz.

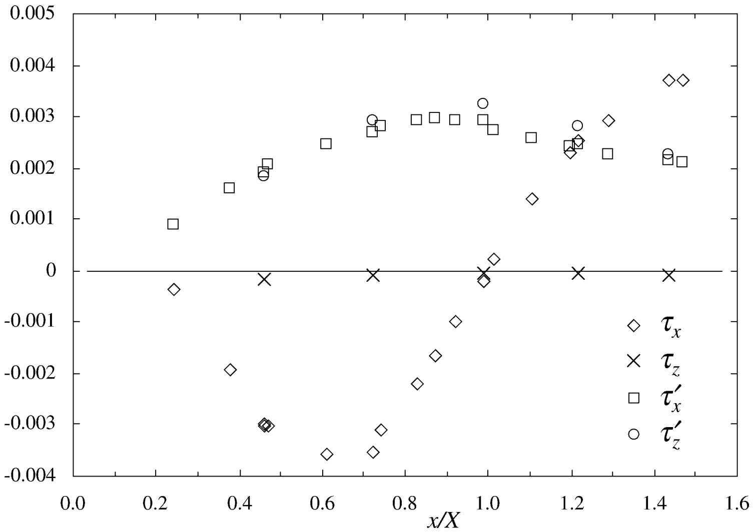

Fig. 1. Coefficients of mean and r.m.s wall shear stress, normalised by $\frac{1}{2}\rho U_r^2$.

3. Present and other measurements, and discussion

3.1. Present measurements

Fig. 1 shows the means and r.m.s. of the fluctuating wall shear stresses, τ_x and τ_z, and τ'_x and τ'_z as measured by the wall-shear-stress probe, as functions of x/X, where these quantities have been normalised by $\frac{1}{2}\rho U_r^2$. The mean lateral stress, τ_z, which ideally would be zero, is acceptably small. In contrast to the earlier measurements of Hancock [8] using the same technique, which showed these two quantities to be equal, τ'_z is slightly larger than τ'_x. However, the Reynolds number is significantly different in the two cases in a range where Reynolds number effects in the outer flow are also significant [13]. Fig. 2 shows U/U_r and $\overline{u^2}/U_r^2$ as functions of y for each of the measurement stations, where the near-wall measurements have been corrected for the gradient error, as discussed in Section 2. (As part of the correction procedure the mean velocity is adjusted beneath $u'_\tau y/\nu = 7$ so that the wall shear stress implied by $\partial U/\partial y$ concurs with that from the wall-shear stress probe.) At reattachment, the bubble height is about 54 mm, the present measurements extending to ~10 mm at each station, though only part of this range need be shown. Both parts of this figure clearly show the effect of viscosity in reducing U and $\overline{u^2}$ to zero beneath y of roughly 1.3 mm, U and $\overline{u^2}$ changing relatively slowly with y further out.

The measurements of Fig. 2(b) are shown again in Fig. 3, this time in the form of Eq. (1.1), where u'_τ/U_r $(= \sqrt{\tau'_x/\rho}/U_r)$ has been taken from the wall shear stress measurements of Fig. 1. Those profiles at stations in the range $0.38 \leqslant x/X \leqslant 1.47$ are seen to fall closely to a single curve, and are certainly within the band of confidence that can be ascribed to these measurements. The bars shown to the left in the figure represent, pessimistically, the error in u'/u'_τ (at $u'/u'_\tau = 4$) arising separately from errors in u'_τ and u', as implied by the largest of the peak-to-peak calibration error bands given in Section 2 for shear stress and velocity. More, typically, the expected error limits are about half these, and indeed this is comparable with the width of the band of data in this figure. The data shown in Fig. 3 exhibit a structural similarity beneath $u'_\tau y/\nu$ of about 70. Although measurements were not made further out than shown, the measurements of Hardman [9] indicate a clear departure from similarity in the outer flow.

Fig. 3 also shows a quadratic viscous sublayer according to

$$u'/u'_\tau \approx u'_\tau y/\nu - a(u'_\tau y/\nu)^2, \tag{3.1}$$

where $a = 0.1$, and a logarithmic behaviour according to

$$u'/u'_\tau = A + B\ln(u'_\tau y/\nu), \tag{3.2}$$

where $A = 2.5$ and $B = 0.5$. At this stage the logarithmic behaviour is presented as an empirical finding. It is of course possible to argue such a behaviour if it is valid to assume that velocity and length scales associated with the flow well away from the wall are not relevant when y is sufficiently small but still large enough for viscous effects to be negligible. That is, that the gradient of r.m.s. velocity, $\partial u'/\partial y$, scales on velocity and length scales of the near-wall turbulence, namely u'_τ and y. This of course follows the very well trodden line of argument for the mean velocity of the canonical boundary layer and channel flows.

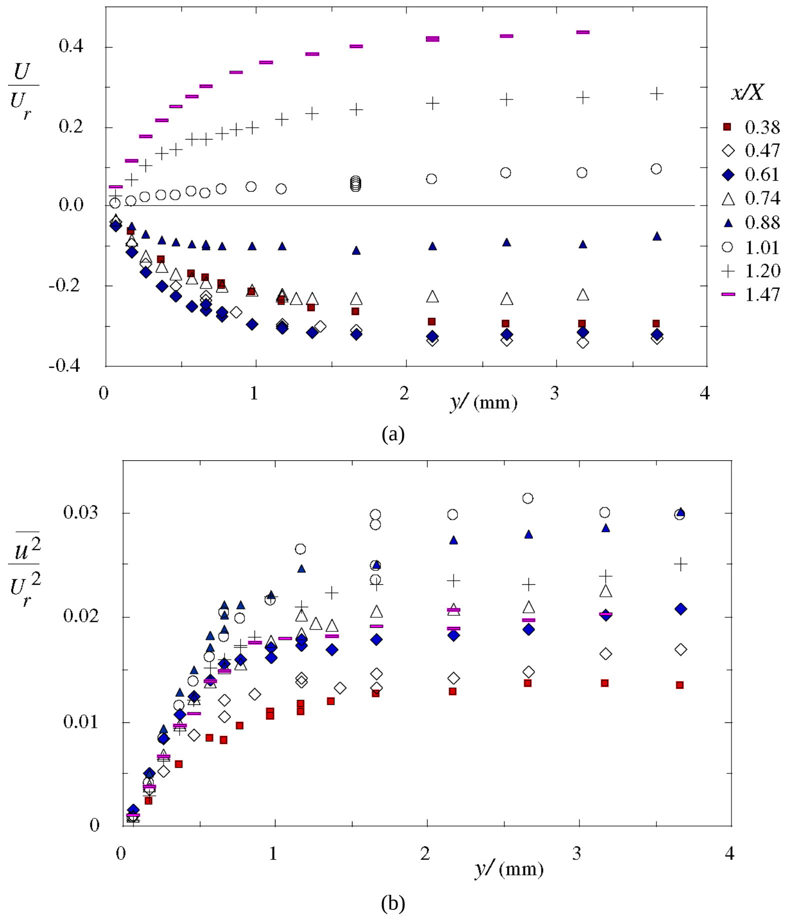

Fig. 2. (a) Mean velocity, U/U_r, in the near-wall layer, as a function of y and x/X. (b) $\overline{u^2}/U_r^2$ in the near-wall layer as a function of y and x/X. Symbols as in (a).

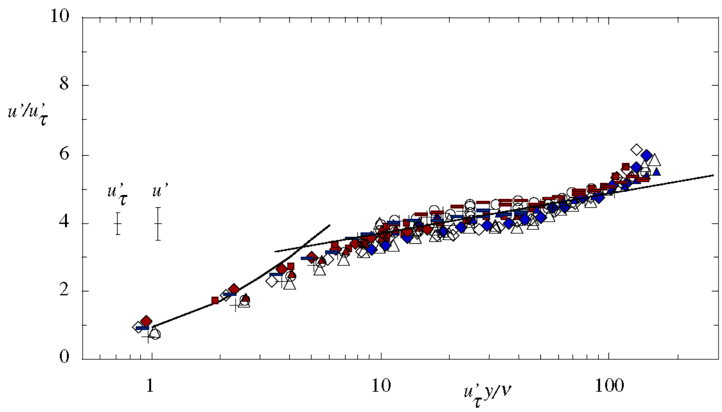

Fig. 3. u'/u'_τ vs $u'_\tau y/\nu$ in semi-logarithmic axes. Symbols as in Fig. 2(a). Other lines are Eqs. (3.1) and (3.2) [16]. Extreme error bars – see text.

In one respect, the present application of this argument is more satisfying in that it involves only turbulence quantities, though it is also true that no reference is made to the mean velocity, which appears to play a passive role.

Indeed, that there is no noticeable effect of the mean velocity in Fig. 3 is a notable point in itself. If, the mean velocity does have no effect, and y and a velocity scale based on the r.m.s. of the wall shear stress fluctuations are the only relevant (length

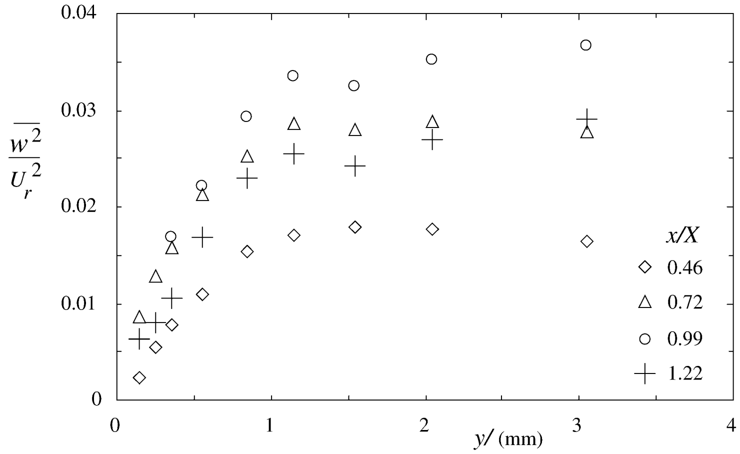

Fig. 4. $\overline{w^2}/U_r^2$ in the near-wall layer as a function of y and x/X.

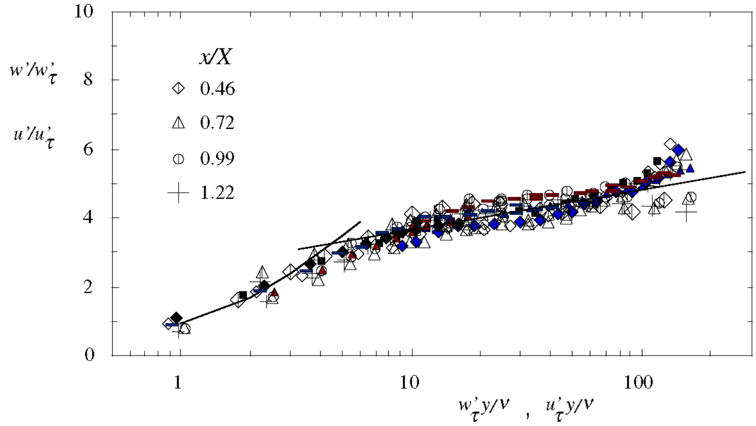

Fig. 5. w'/w'_τ vs $w'_\tau y/\nu$ in semi-logarithmic axes, and data of Fig. 3.

and velocity) scales, then it would be anticipated that the lateral velocity fluctuations, w', would scale according to Eq. (1.2). Fig. 4 shows $\overline{w^2}$ as a function of y and, as in Fig. 2(b), viscous effects are seen beneath y of roughly 1.3 mm. Fig. 5 shows the same data but now in terms of w'/w'_τ as a function of $w'_\tau y/\nu$ at four stations, together with data from Fig. 3, where w'_τ has been obtained from τ'_z given in Fig. 1. To within the uncertainty of the measurements there is no distinction to be drawn between the two sets beneath $w'_\tau y/\nu$, $u'_\tau y/\nu \approx 70$. There is a trend of w'/w'_τ lying slightly above u'/u'_τ, but this is within the uncertainty of the measurements, and there is no trend with position. To within the expected errors Eqs. (1.1) and (1.2) represent identical functional relationships. As for u' (Eq. (3.2)), a logarithmic form for w' follows if $\partial w'/\partial y$ scales only on w'_τ and y. The lines given in Fig. 3 are also given in Fig. 5. Further out, u' and w' are different, with u' clearly larger then w'.

A quadratic viscous sub-layer behaviour comes from supposing a sinusoidally oscillating flow above, imposed by the outer flow [16]; the quadratic form is the first two terms. Even as close as $u'_\tau y/\nu = 1$, and taking $a = 0.1$ as typical, u'/u'_τ is 0.9, and so there is no significant region of a *linear* viscous sublayer. A buffer layer could be said to exist between $\sim 2 < u'_\tau y/\nu$, $w'_\tau y/\nu < \sim 10$. As noted in Section 2, the error arising from high instantaneous velocity gradients is only significant beneath $u'_\tau y/\nu = 10$ or less, and beneath $u'_\tau y/\nu = 3$ for some stations. Therefore, the concurrence seen above $u'_\tau y/\nu$ (and $w'_\tau y/\nu) = 10$ or less in Figs. 3 and 5 is independent of this error and the associated correction.

Finally, as a footnote concluding this section, it should perhaps be mentioned that because of the familiar form it is tempting to compare the accuracy of the measurements in Figs. 3 and 5 with that achieved for the mean velocity in boundary layers. It must be remembered that the former are considerably harder to make to the same level of accuracy, which is why the errors here are larger. The current departure from a precise collapse is consistent with the expected error limits in measuring the intensities of the velocity the wall shear stress fluctuations.

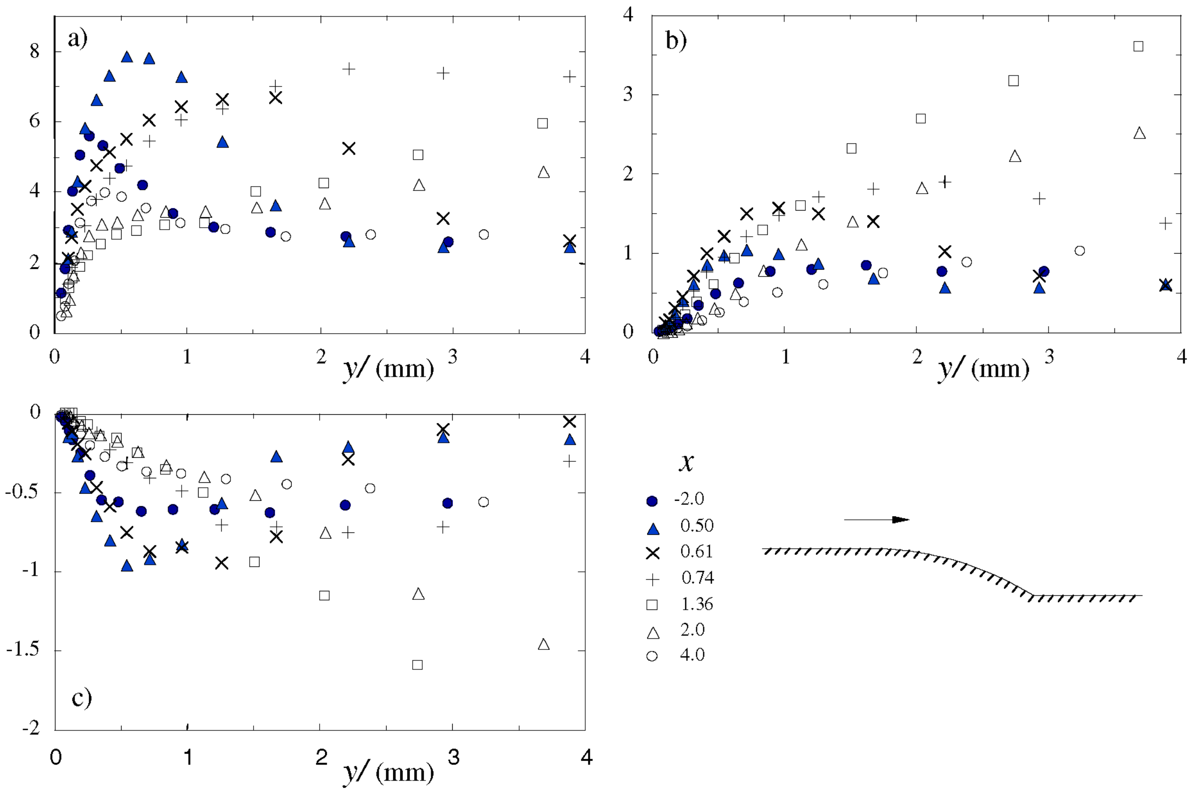

Fig. 6. Reynolds stress profiles of Song et al. [11] over backward-curved step, (a) $\overline{u^2}/u^2_{\tau\mathrm{ref}}$, (b) $\overline{v^2}/u^2_{\tau\mathrm{ref}}$ and (c) $\overline{uv}/u^2_{\tau\mathrm{ref}}$.

3.2. Measurements of Song et al.

Song et al. [11] made measurements of $\overline{u^2}$, $\overline{v^2}$ and $\overline{uv}$ for a thick turbulent boundary layer separating from the curved backward-facing step, as shown in Fig. 6. The upstream boundary layer (0.99) thickness was about 0.6 of the bubble length, and so the initial conditions are therefore very different from the sharp-edge separation of a very thin laminar boundary layer in the present flow. In their data set x is zero at the start of the curvature and 1 at the corner. The measurements were made at stations upstream of and near mean separation ($x \approx 0.77$) and at and downstream of reattachment ($x \approx 1.36$), along vertical traverse lines. For the present purposes, where the surface is curved, the Reynolds stresses have been resolved into axes rotated to the local surface direction. One set of data, that at $x = 1$, is not used because of ambiguity of direction at the corner. In that turbulent separation from a smooth surface is spatially intermittent it is at least legitimate to suppose that it might have some features similar to that beneath and near reattachment, and on this basis measurements at and upstream of separation are included here. Although this flow is substantially different from the present flow just discussed there is, as will be seen, close agreement in the behaviour of the near-wall layer.

Their data, reproduced in Fig. 6, is normalised by a reference friction velocity, $u_{\tau\mathrm{ref}}$, taken at the upstream-most station ($x = -2$, where the Reynolds number based on momentum thickness was 3500). Fig. 7(a) shows u' from 6(a) normalised, instead, in terms of u'_τ, together with the two trend lines (a quadratic sublayer and a 'log-law') from Fig. 3 to aid comparison. Here, u'_τ has been determined, by *extrapolation*, from the first few points in each profile nearest the surface, by rewriting Eq. (3.1) as $(u'/u'_\tau)/(u'_\tau y/\nu) = 1 - au'_\tau y/\nu$ and adjusting u'_τ and a for best fit; u'_τ is given directly by this fitting procedure applied to the first few points. The agreement with the present results is remarkably good, given that it is dependent on differentiation over a few measurements in each case, and on extrapolation – and highly dependent on measurement accuracy.

Fig. 7(b) shows the same data (for three profiles) but now with the u'_τ obtained so as to give closer agreement with the 'log-law' trend line. This is like the Clauser chart method for calculating mean wall shear stress from the mean velocity profile. As a procedure it gives broadly uniform weighting of importance to each point below $u'_\tau y/\nu$ of about 70, and exhibits a uniform degree of scatter, which adds to the justification of adjusting u'_τ in this way. From some of the data points, assuming the real behaviour is a smooth variation, one can see a degree of variation between some adjacent points that gives an uncertainty in the

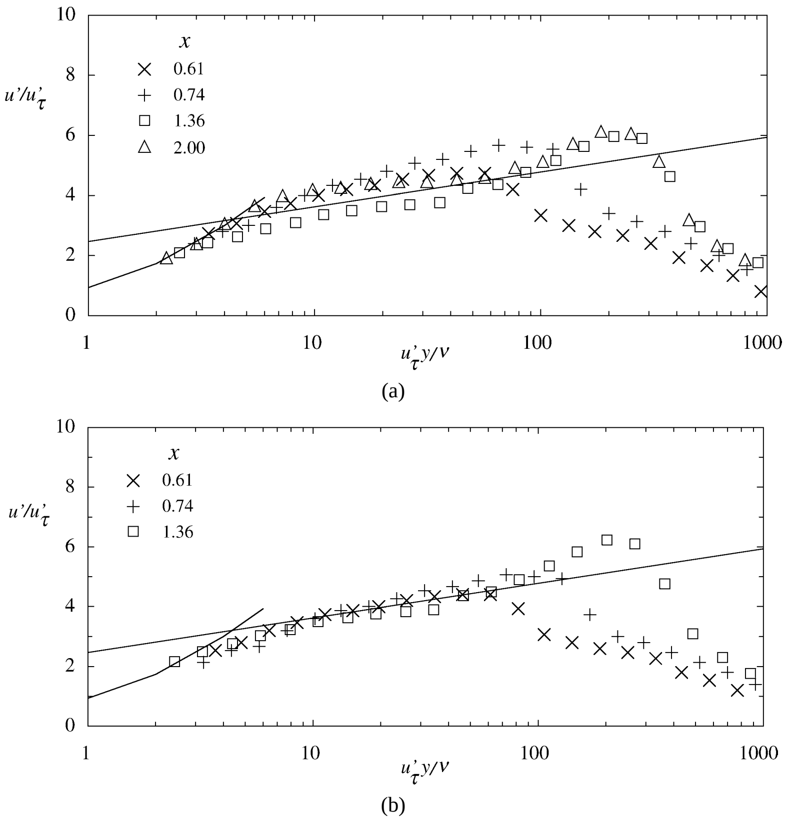

Fig. 7. (a) Song's measurements (beneath and near bubble) in new scaling. Other lines as in Fig. 3. (b) Song's measurements for adjusted u'_τ cases – see text. Other lines as in Fig. 3.

slope that would explain the greater spread seen in Fig. 7(a). For this reason, Fig. 7(b) is regarded as the more reliable. $u'_\tau/u_{\tau\mathrm{ref}}$ as used in both figures is given in Table 1.

The concurrence in these three profiles (Fig. 7(b)), two near separation (rather than just around reattachment), and the concurrence with the present measurements is remarkable, adding strong support to the original conjecture that the velocity scale as defined here is a relevant scale for the near-wall turbulent motion. Moreover, the fact that the flow of Fig. 7 was formed from a separating *turbulent* boundary layer, adds further support to the view (initially based on Figs. 3 and 5) that the near-wall layer beneath a separated flow, so scaled, is independent of the outer flow.

Figs. 8(a) and 8(b) show, respectively, the velocities v' and s' in the scaling of Eqs. (1.3) and (1.4), from Song's measurements. As noted in the introduction, v'_0 and s'_0 do not have the immediate connection with other quantities, unlike u'_τ and w'_τ. The essence of Eqs. (1.3), and similarly (1.4), is that a velocity scale may be found at each x-station which will cause the corresponding profiles of v' to fall on a single curve, and likewise for s'. This is the procedure that has been used here – where an arbitrary factor is involved, as discussed shortly. Remarkably, and unexpectedly, the collapse was also found to apply to the profiles in both the upstream boundary layer and in the boundary layer developing downstream. Both figures show a collapse beneath $v'_0 y/\nu$ of 30 and beneath $s'_0 y/\nu$ of 20, irrespective of the conditions further out, allowing the collapse to be described, at least provisionally, as 'universal'. As will be seen in Subsection 3.3 below, u'/u'_τ is clearly not a universal function of $u'_\tau y/\nu$, and so the quite remarkable behaviour displayed in Fig. 8 was even less anticipated than that already exhibited in Figs. 3, 5 and 7.

As just mentioned, there is an arbitrary factor involved in choosing v'_0, and similarly s'_0. Supposing the behaviour conforms to Eq. (1.3), then if all v'_0 are multiplied by some factor, f say (in effect, to make new v'_0), the resulting behaviour will still be of the form given by Eq. (1.3). For convenience, v'_0 and s'_0 have been chosen so that in the upstream boundary layer ($x = -2$) they are equal to $u_{\tau\mathrm{ref}}$, the mean wall shear stress friction velocity. Values of $v'_0/u_{\tau\mathrm{ref}}$ and $s'_0/u_{\tau\mathrm{ref}}$ are given in Table 1.

Figs. 8(a) and 8(b) also show 'log-law' lines and the simulation results of Spalart [21], (where, for the latter, v'_0/u_τ and s'_0/u_τ are unity). The log-law lines shown are given by,

$$v'/v'_0 = A_v + B_v \ln(v'_0 y/\nu) \quad \text{and} \quad s'/s'_0 = A_s + B_s \ln(s'_0 y/\nu), \tag{3.3,3.4}$$

Table 1
Inferred velocity scales. Song et al.: ( ) denotes u'_τ used in Fig. 7(b); other u'_τ determined from extrapolation of first few points. (See text.)

Song et al. x'	$u'_\tau/u_{\tau\mathrm{ref}}$	$v'_0/u_{\tau\mathrm{ref}}$	$s'_0/u_{\tau\mathrm{ref}}$	
−2	0.66	1.00	1.00	
0	0.67	1.00	1.08	
0.50	0.63	1.33	1.06	
0.61	0.65 (0.70)	1.46	0.97	
0.74	0.58 (0.65)	1.30	0.69	
1.36	0.57 (0.55)	1.08	0.62	
2	0.50	0.90	0.64	
4	0.53	0.80	0.80	
7	0.54	0.90	0.85	
Spalart Re_θ	u'_τ/u_τ	v'_0/u_τ	w'_τ/u_τ	s'_0/u_τ
1410	0.650	1	0.545	1
Moser et al. h^+	u'_τ/u_τ	v'_0/u_τ	w'_τ/u_τ	s'_0/u_τ
590	0.637	1	0.511	1
Le et al. x/h	u'_τ/U_0	v'_0/U_0	w'_τ/U_0	s'_0/U_0
−3	0.0345	0.047	0.0230	0.051
4	0.0330	0.067	0.0325	0.033
6	0.0345	0.070	0.0350	0.045
10	0.0317	0.056	0.0290	0.048
15	0.0303	0.048	0.0252	0.046

where, respectively, A_v and B_v are -0.82 and 0.5, and A_s and B_s are -0.55 and 0.5. The slopes of these purely empirical lines appear to provide a reasonable representation in the outer parts of the 'universal' regions (i.e. the outer parts of Eqs. (1.3) and (1.4)), before the various profiles start to diverge above the near-wall layer. Of course, logarithmic forms follow if $\partial v'/\partial y$ scales only on v'_0 and y – and likewise for s'. That the slopes are also 0.5 is fortuitous in that they are dependent on the factor f, mentioned above.

3.3. Boundary layer flow

As already said, Fig. 8 clearly shows v' and s' to follow an apparently universal scaling irrespective of the external flow. This is not the case for u', as can be seen from Fig. 9, which shows profiles upstream of separation ($x = -2$ and 0.5), profiles after reattachment ($x = 2, 4$ and 7), and that at reattachment ($x = 1.36$). Each of these profiles is presented with u'_τ evaluated from extrapolation of the first few points, as in Fig. 7(a). (Exactly the same conclusions would follow had the adjusted u'_τ been used for the profile at $x = 1.36$.) Comparing the profiles (of Fig. 9) at $x = 1.36$ and 2 shows the redevelopment of the peak at $u'_\tau y/\nu$ of about 10, but with virtually no difference above $u'_\tau y/\nu$ of about 50. A $u'_\tau y/\nu$ of 10 is equivalent to $u_\tau y/\nu$ of 15 in a canonical boundary layer, and it is presumed that the development (or redevelopment in this case) of the peak is associated with the rise in generation of $\overline{u^2}$ and with the development of the structures characteristic of the standard inner layer. This height corresponds to $v'_0 y/\nu$ and $s'_0 y/\nu$ of $\sim$15 (in the canonical layer) and to where the turbulent kinetic energy production is at a peak, and so it is noteworthy that there is no noticeable affect seen in v' or s' in Fig. 8. Streamwise vortical structures in the inner layer are associated with the transfer of streamwise momentum towards and away from the surface, contributing primarily to the second and forth of the $u - v$ quadrants and to the creation of the main contribution to $\overline{uv}$, as well as contributing to $\overline{v^2}$. (For reviews of near-wall structures see, for example, Robinson [5] and, more recently, Tomkins and Adrian [22].) One conjecture has to be that development of these structures is such that the whole of the near-wall layer is influenced in a way that v' and s' still conform to Eqs. (1.3) and (1.4), and that only the velocity scales v'_0 and s'_0 are changed as a result. While this would be both significant and surprising, the absence of any influence on v' and s' would be even more so.

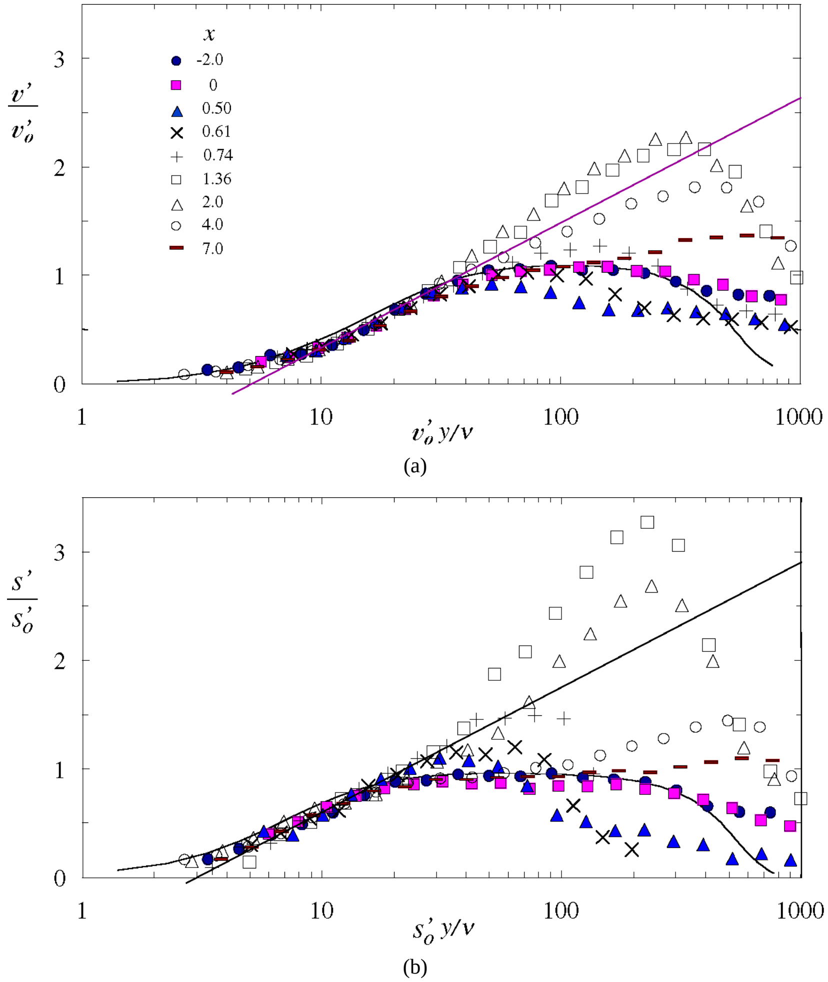

Fig. 8. (a) v' from Song et al. in the scaling of Eq. (1.3). Other lines are data of Spalart [21] and Eq. (3.3). (b) s' from Song et al. in the scaling of Eq. (1.4). Symbols as in Fig. 8(a). Other lines are data of Spalart [21] and Eq. (3.4).

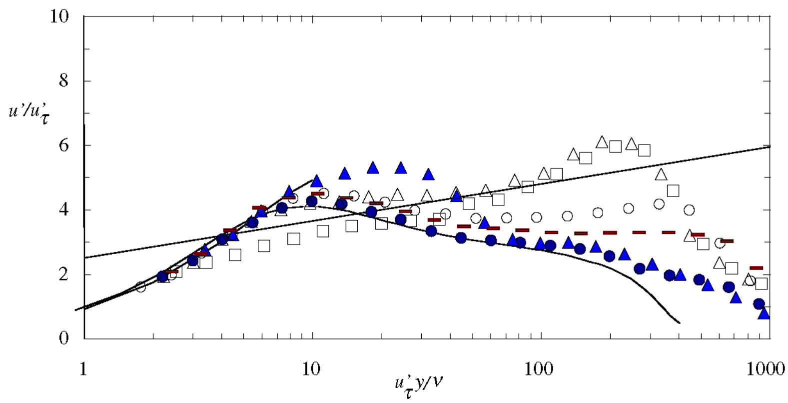

Fig. 9. u' from Song et al. in the scaling of Eq. (1.1), upstream and downstream of the bubble. Symbols as in Fig. 8(a). Other lines are data of Spalart [21], and as in Fig. 3.

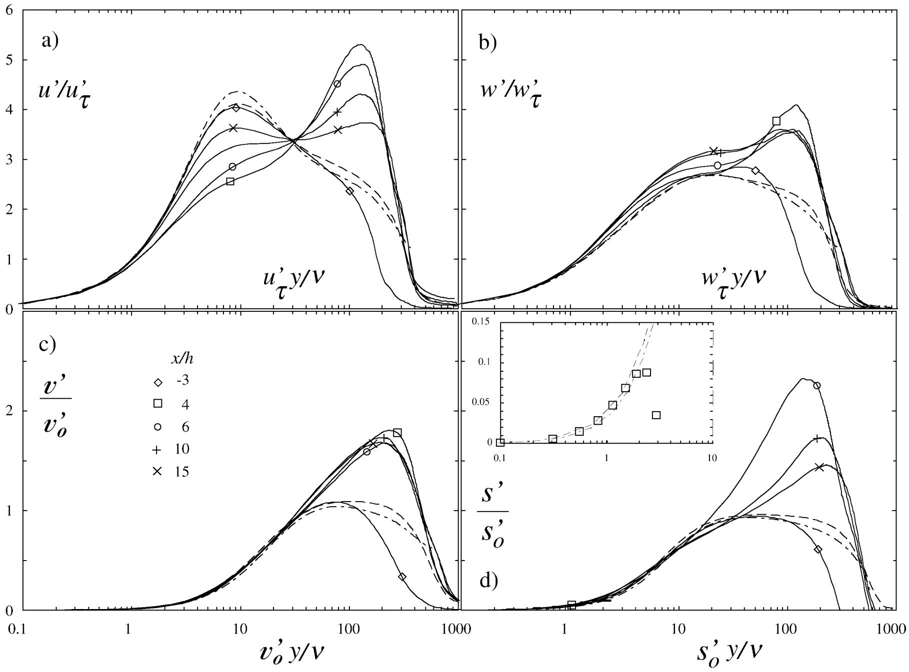

Fig. 10. Simulation data of Le et al. [12]. (a) u'/u'_τ vs $u'_\tau y/\nu$; (b) w'/w'_τ vs $w'_\tau y/\nu$; (c) v'/v'_0 vs $v'_0 y/\nu$; (d) s'/s'_0 vs $s'_0 y/\nu$. Inset in (d) is at $x/h = 4$ (see text). Other lines are data of Spalart [21] and Moser et al. [23].

The profile of u'/u'_τ at $x = 0.5$ (Fig. 9) shows a marked amplification of the peak (with respect to that at $x = -2$) before its subsequent disappearance by $x = 0.61$ (as can be seen in Fig. 7). This peak in u'/u'_τ (at $x = 0.5$) is at about $u'_\tau y/\nu = 20$, which at this station corresponds to $v'_0 y/\nu$ of about 40 and $s'_0 y/\nu$ of about 30. But, as can be seen from Fig. 8, there is again no affect on v' or s', at least in terms of a corresponding peak. It is interesting to note, too, that above $u'_\tau y/\nu$ of about 80 the r.m.s. velocity, u'/u'_τ, is as in the unperturbed boundary layer at $x = -2$. This resembles the comparison made above between the profiles at $x = 1.36$ and $x = 2$, marking the reappearance of the peak. In both cases the changes between these pairs of stations is confined to an inner layer. In contrast, the same sort of behaviour, of an inner-layer peak disappearance and reappearance, is not seen in v'/v'_0 or s'/s'_0 (Fig. 8).

3.4. Back-step flow of Le et al.

Another test is provided by the direct numerical simulations of Le et al. [12], for a turbulent boundary layer, albeit at a low momentum thickness Reynolds number of 667, separating from a backward-facing step. The profiles, including those for the lateral fluctuations (w'), are shown in Fig. 10, where u'_τ and w'_τ have been obtained from u' and w' at small y. These figures include the DNS results of Spalart [21], as in preceding figures, and also of Moser et al. [23]. Reattachment is at $x/h = 6$ where h is the step height and x is measured from the step. Figs. 10(c) and 10(d) show good agreement with the measurements of Song et al., though the upper limit of collapse is less, at $v'_0 y/\nu \approx 25$ and $s'_0 y/\nu = 10$. It is supposed that this is a consequence of the lower Reynolds number of this flow (as can be seen from the lower $v'_0 y/\nu$ and $s'_g y/\nu$ at which v' and s' fall to zero in the free stream.) In contrast, the profiles of u' (and likewise w') fall well below both the present measurements and those of Song, and it is again supposed that this is also a consequence of the low Reynolds number. At $x/h = 4$, i.e. upstream of reattachment, there is a very small region of positive $\overline{uv}$. The profile of s' for this case is shown in the inset in Fig. 10(d), where the departure from the sublayer form (broken lines) at $s'_0 y/\nu$ of about 2 is a consequence of there being only a very small extent of positive uv at this station. Beneath this height the agreement is remarkably good.

4. Further discussion and concluding comments

The present measurements and those of Song et al. [11] provide strong support for the scaling of the Reynolds stresses in the near-wall region beneath the bubble according to Eqs. (1.1) to (1.4). These two sets of measurements show a high degree

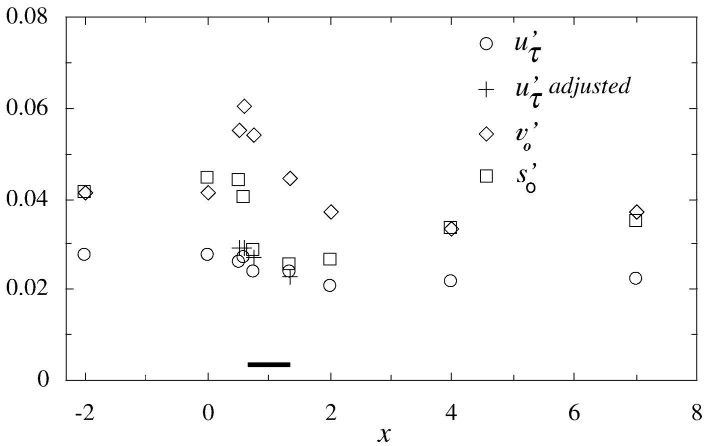

Fig. 11. Development of velocity scales for Song et al. [11]. Normalised by free-stream velocity at $x = -2$.

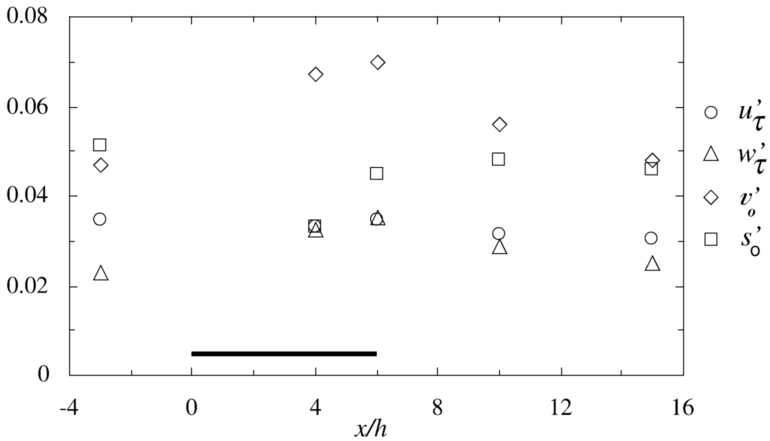

Fig. 12. Development of velocity scales for Le et al. [12]. Normalised by free-stream velocity at $x/h = -3$.

of agreement even though the flows differ substantially – most notably at and near separation. Indeed, Song's measurements show the same scaling to apply upstream of and at separation of a turbulent boundary layer from a smooth wall, independent of flow conditions further out, as well as through reattachment. However, these results suggest that the distance over which this near-wall scaling applies, in terms of the bubble overall height, does depend on the outer flow conditions (and, it appears, on Reynolds number as would be expected). This distance for the u' profile was roughly 0.1 bubble heights at attachment, while in Song's flow it was roughly 0.05.

Quite unexpectedly, and quite remarkably, v' and s' exhibit an apparently universal behaviour beneath the whole of the bubble and in standard and developing (or relaxing) boundary layers. The simulations of Le et al. [12], for a turbulent boundary layer separating from a back step also show good agreement of v' and s' with the above results, u' beneath the bubble is markedly lower than in Song's or in the present measurements and, tentatively, this is attributed to the low Reynolds number of the simulation having a larger effect on u' than on either v' or s'. Overall, the fact that v' and s' behave in an apparently universal manner, but that u' does not, poses some interesting questions regarding the near-wall structures. It appears the behaviour of u' may be linked with the disappearance and reappearance of the near-wall streaks [7].

The change in the velocity scales with the flow development gives an indication of the change taking place in the near-wall layer. The variation in u'_τ and w'_τ for the present measurements is given in Fig. 1, albeit as τ'_x and τ'_z. Figs. 11 and 12 show, respectively, the velocity scales for Song et al. and Le at al., where the horizontal bar in each figure indicates the bubble mean length. Fairly dramatic changes can be seen in Fig. 11 for v'_0 and s'_0 , the first showing a rapid rise and the latter a rapid fall, with both returning much more slowly to about the same proportion of u'_τ as in the upstream layer by $x = 4$, if not before. In contrast, u'_τ shows a much more gradual and smaller variation. It is of course true that these data lack detail within the bubble, for v' and s'. However, the apparently universal behaviour of these quantities upstream of and at separation, at reattachment and downstream, and in the canonical boundary layer, suggests v' and s' might behave the same way beneath the whole of the bubble.

Song et al. note that in the inner layer their profile at $x = 7$ falls close to that at $x = -2$, once the scaling of DeGraaff and Eaton [1] is used, reinforcing, they argue, the case for that scaling. Fig. 9 includes these two profiles, but in the current framework, where the two can be seen also to fall close to each other beneath $u'_\tau y/\nu$ of about 100. Their scaling [1] is only formally consistent with the present one where the velocity scales are in constant proportion. The present approach has the advantage of involving only one rather than two velocity scales. Further investigation is needed.

Finally, the constancy of the scaling beneath and near the bubble and the apparently passive role played by the mean (convection) velocity suggests the behaviour might be equivalent to the 'box of turbulence' conceptualisation, where there is no mean velocity (relative to the walls). Other than to make this point this is not pursued further here.

Acknowledgements

The author is particularly grateful to Dr. Simon Song for making his measurements available in electronic form.

References

[1] D. De Graaff, J.K. Eaton, Reynolds-number scaling of the flat-plate turbulent boundary layer, J. Fluid Mech. 422 (2000) 319–346.
[2] M. Metzger, J. Klewicki, K. Bradshaw, R. Sadr, Scaling the near-wall axial turbulent stress in the zero pressure gradient boundary layer, Phys. Fluids 13 (2001) 1819.
[3] H.H. Fernholz, P.J. Finley, The incompressible zero-pressure-gradient turbulent boundary layer: an assessment of the data, Prog. Aerospace Sci. 32 (1996) 245–311.
[4] A.A. Townsend, The Structure of Turbulent Shear Flow, Cambridge University Press, 1976.
[5] S.K. Robinson, Coherent motions in the turbulent boundary layer, Ann. Rev. Fluid Mech. 23 (1991) 601–639.
[6] H.H. Fernholz, Near-wall phenomena in turbulent separated flows, Acta Mech. 4 (Suppl.) (1994) 57–67.
[7] Y. Na, P. Moin, Direct numerical simulation of a separated turbulent boundary layer, J. Fluid Mech. 374 (1998) 379–405.
[8] P.E. Hancock, Measurements of mean and fluctuating wall shear stress beneath spanwise-invariant separation bubbles, Exp. Fluids 27 (1999) 53–59.
[9] J.R. Hardman, Moderately three-dimensional separated and reattaching turbulent flow, PhD Thesis, University of Surrey, 1998.
[10] P.E. Hancock, Scaling of the near-wall layer beneath reattaching separated flow, in: A.J. Smites (Ed.), IUTAM Symposium on Reynolds Number Scaling in Turbulent Flow, September 2002, ISBN 1-4020-1775-8, Kluwer Academic, Princeton, 2003.
[11] S. Song, D.B. DeGraaff, J.K. Eaton, Experimental study of a separating, reattacing, and redeveloping flow over a smoothly contoured ramp, Int. J. Heat and Fluid Flow 21 (2000) 512–519.
[12] H. Le, P. Moin, J. Kim, Direct numerical simulation of turbulent flow over a backward-facing step, J. Fluid. Mech. 330 (1997) 349–374.
[13] P.E. Hancock, Low Reynolds number two-dimensional separated and reattaching turbulent shear flow, J. Fluid Mech. 410 (2000) 101–122.
[14] F. Ciampoli, P.E. Hancock, Effects of flow width in nominally two-dimensional turbulent separated flows, Exp. Fluids, submitted for publication.
[15] M. Schober, P.E. Hancock, H. Siller, Pulsed-wire anemometry near walls, Exp. Fluids 25 (1998) 151–159.
[16] P.E. Hancock, Pulsed-wire measurements in the near-wall layer in a reattaching separated flow, Exp. Fluids 37 (2004) 323–330.
[17] I.P. Castro, M. Dianat, Pulsed-wire velocity anemometry near walls, Exp. Fluids 8 (1990) 343–352.
[18] I.P. Castro, M. Dianat, L.J.S. Bradbury, The pulsed-wire skin-friction measurement technique, in: Turbulent Shear Flows, vol. 5, Springer-Verlag, 1987, pp. 278–290.
[19] V.C. Patel, Calibration of the Preston tube and limitations on its use in pressure gradients, J. Fluid. Mech. 23 (1965) 185–208.
[20] I.P. Castro, B.S. Cheun, The measurement of Reynolds stresses with a pulsed-were anemometer, J. Fluid Mech. 118 (1982) 41–58.
[21] R.P. Spalart, Direct simulation of a turbulent boundary layer up to $Re_\theta = 1410$, J. Fluid Mech. 187 (1988) 61–98.
[22] C.D. Tomkins, R.J. Adrian, Spanwise structure and scale growth in turbulent boundary layers, J. Fluid Mech. 490 (2003) 37–74.
[23] R.D. Moser, J. Kim, N.N. Mansour, Direct numerical simulation of turbulent channel flow up to $Re = 590$, Phys. Fluids (4) 11 (1999) 943–945.